2004

Automatic Regional Moment Tensor Inversion in the European-Mediterranean Region

Fabrizio Bernardi
Swiss Seismological Service

Jochen Braunmiller
Swiss Seismological Service, jbraunmiller@usf.edu

Urs Kradolfer
Swiss Seismological Service

Domenico Giardini
Swiss Seismological Service

Geophys. J. Int. (2004) **157,** 703–716 doi: 10.1111/j.1365-246X.2004.02215.x

Automatic regional moment tensor inversion in the European-Mediterranean region

Fabrizio Bernardi, Jochen Braunmiller, Urs Kradolfer and Domenico Giardini

Swiss Seismological Service, Institute of Geophysics, ETH Zürich, 8093 *Hönggerberg, Switzerland. E-mail: fabrizio@seismo.ifg.ethz.ch*

Accepted 2003 November 18. Received 2003 November 18; in original form 2003 May 5

SUMMARY

We produce fast and automatic moment tensor solutions for all moderate to strong earthquakes in the European-Mediterranean region. The procedure automatically screens near real-time earthquake alerts provided by a large number of agencies. Each event with magnitude $M \geq 4.7$ triggers an automatic request for near real-time data at several national and international data centres. Moment tensor inversion is performed using complete regional long-period (50–100 s) waveforms. Initially the data are inverted for a fixed depth to remove traces with a low signal-to-noise ratio. The remaining data are then inverted for several trial depths to find the best-fitting depth. Solutions are produced within 90 min of an earthquake. We analyse the results for the period 2000 April to 2002 April to evaluate the performance of the procedure. For quality assessment, we compared the results with the independent Swiss regional moment tensor catalogue (SRMT), and divided the 87 moment tensor solutions into three groups: 38 A-quality solutions with well-resolved M_w, depth and focal mechanism; 21 B-quality solutions with well-resolved M_w; and 28 unreliable C-quality solutions. The non-homogeneous station and event distributions, varying noise level, and inaccurate earthquake locations affected solution quality. For larger events ($M_w \geq 5.5$) we consistently obtained A-quality solutions. For $M_w = 4.5$–5.5 we obtained A- and B-quality solutions. Solutions that pass empirical rules mimicking the *a posteriori* quality for our data set are automatically disseminated.

Key words: broad-band seismology, European-Mediterranean region, magnitude, moment tensor inversion, real-time source parameters, regional surface waves.

1 INTRODUCTION

Quick and accurate source parameter determination (magnitude, depth and focal mechanism) provides important information for fast intervention in areas badly damaged by large earthquakes. When compared to standard determination of earthquake location and magnitude, moment tensor inversion usually provides more accurate source parameters and particularly so for the size of large events, since their moment magnitudes M_w do not saturate (Kanamori 1977). The recent increase in the number of near real-time accessible broad-band stations in the European-Mediterranean region now allows automatic, near real-time moment tensor analysis for monitoring strong events.

Accurate and quick moment tensor inversion is routinely performed on a global scale by the Harvard Centroid-Moment Tensor (CMT) project (Dziewonski *et al.* 1981; Dziewonski & Woodhouse 1983), the United States Geological Survey (Sipkin 1982, 1986) and the Earthquake Research Institute (ERI), Japan (Kawakatsu 1995). These approaches use teleseismic data, limiting analysis to stronger earthquakes ($M_w \geq 5.5$). Analysis of smaller earthquakes requires data recorded at regional distances, which is becoming possible with the growing number of broad-band seismic networks. Several groups in the United States (Dreger & Helmberger 1993; Ritsema & Lay 1993; Romanowicz *et al.* 1993; Nábělek & Xia 1995; Braunmiller *et al.* 1995; Thio & Kanamori 1995; Dreger *et al.* 1995; Pasyanos *et al.* 1996) and Japan (Kubo *et al.* 2002) routinely invert for the seismic moment tensor using seismic data recorded at near regional distances ($\Delta \leq 10^\circ$).

In the European-Mediterranean region, event–station distances are generally larger ($\Delta \geq 10^\circ$) than in the western United States. Several studies (Arvidsson & Ekström 1998; Braunmiller 1998), however, have shown that source parameters of moderate events can be determined routinely with long-period regional data ($T \geq 30$–40 s) for larger event–station distances. The Swiss Seismological Service (Braunmiller *et al.* 2000, 2002) and the Italian Istituto Nazionale di Geofisica e Vulcanologia (INGV) (Pondrelli *et al.* 2002) now routinely produce moment tensor solutions in the European-Mediterranean area for moderate to strong earthquakes ($M_w \geq 4.5$), and smaller earthquakes ($M_w \geq 3.0$) in the Alpine area (Braunmiller *et al.* 2000, 2002). Small to moderate earthquakes in the western Mediterranean region are regularly processed by the Spanish Instituto Andaluz de Geofísica (Stich *et al.* 2003).

Here we test whether the current near real-time data availability and location accuracy are sufficient for automatic regional moment tensor retrieval using intermediate- to long-period surface waves (50–100 s). Our goal is to develop a robust procedure that provides

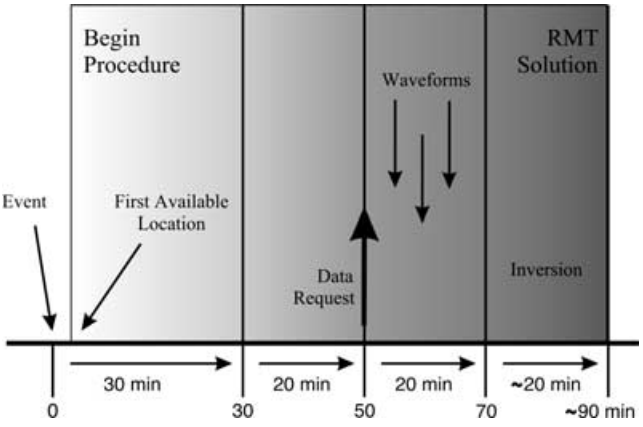

Figure 1. Sketch of the automatic moment tensor inversion procedure. The procedure is triggered when an earthquake alert indicates an event with magnitude $M \geq 4.7$ in the European-Mediterranean region (22°–68°N, 25° W–60°E). Data requests are sent 50 min after the origin time: 30 min correspond to the waveform length used for analysis, and we wait for an additional 20 min to ensure data availability. After a further 20 min, data acquisition is considered complete and inversion starts, resulting in an automatic moment tensor solution within 90 min of an event.

fully automatic, fast and reliable solutions for moderate to strong earthquakes in the European-Mediterranean region.

Our automatic procedure consists of two main parts: first, moment tensor inversion for a detected earthquake; and second, automatic quality assessment of the solution. We first describe the method and show the reliability of the automatic solutions. Then we present empirical rules for automatic quality assessment. Finally, we discuss source parameters (focal mechanism, depth and M_w) and investigate factors that affect solution quality.

2 DATA AND METHOD

Ultimately, we would like to obtain a moment tensor within a few minutes of an event. This requires on-line data access to stations at close epicentral distances, which is currently unavailable for most of our study region. We anticipate that present waiting periods arising from sparse networks and time delays for data acquisition will shorten considerably in the future.

2.1 Data acquisition

Automatic moment tensor inversion consists of several steps (Fig. 1). A few minutes after an event, an automatic earthquake alert (location, magnitude) is generally available, provided by the Swiss Seismological Service (SED) and other agencies linked to this institute. Automatic information coming from many agencies may include false alarms, but guarantees that no significant event is missed. We screen incoming information, and any event in the European-Mediterranean area ($22^\circ \leq$ Lat $\leq 68^\circ$, $-25^\circ \leq$ Long $\leq 60^\circ$) with magnitude $M \geq 4.7$, independent of magnitude type (M_L, m_b, M_S), starts the routine automatically.

We invert complete broad-band waveforms recorded at regional epicentral distances ($\Delta \leq 20^\circ$); therefore, our data window is 30 min long. We wait an additional 20 min to assure data availability (Fig. 1) before sending data requests to the AutoDRM (Kradolfer 1996) of several international (ORFEUS, USGS) and national data centres (in Austria, Czech Republic, Germany, Israel, Norway, Switzerland) that provide near real-time broad-band seismograms. The data centres automatically process these requests, and, usually within 20 min, all available seismograms are received at our server to be stored and prepared for inversion. 70 min after the event origin time, data acquisition is considered complete and the inversion starts, resulting in an automatic moment tensor solution within 90 min of an earthquake.

Between 2000 April and 2002 April only stations in central and northern Europe, Israel, the Caucasus region and Russia provided near real-time data (black triangles in Fig. 2). Data availability and the response time of data centres varied. To ensure that we received a sufficient number of seismograms, we chose a relatively long waiting period before requesting data and starting the inversion. Stations in the western and central Mediterranean Sea, Turkey and eastern Europe (white triangles in Fig. 2) became available during mid-2002 and are only shown to illustrate the evolving and improving station coverage.

2.2 Algorithm

The algorithm uses intermediate- to long-period three-component regional data. The inversion code, described in Giardini (1992), has already been applied to many earthquakes (Giardini 1992; Giardini *et al.* 1993a,b; Sicilia 1999). Synthetic seismograms are generated by normal-mode summation (Woodhouse 1988) computed for the PREM earth model (Dziewonski & Anderson 1981) at various source depths and stored in libraries for quick access. The moment tensor is constrained to be deviatoric. We do not invert for the source centroid but compute time corrections by re-aligning data and synthetics (Giardini 1992). Depth is retrieved by minimizing the normalized variance (defined as the ratio of variance to data vector norm) for various trial depths.

2.3 Inversion

The moment tensor inversion automatically starts 70 min after an event (Fig. 1). The alert is the first available location, which is not necessarily the best epicentre estimate. 70 min after an event, several automatic and/or manual locations are usually available and we choose the *a priori* most accurate. We prefer a location from a network that surrounds the epicentre. When that is not available, we look for a manual location or one provided by an agency with a large aperture network.

The seismograms are bandpass-filtered between 50 and 100 s period. A low-pass filter at 50 s applied to regional seismograms minimizes the effect of inaccurately known propagation paths and allows moment tensor retrieval of moderate-sized earthquakes ($M_w \geq 4.5$) with a simple average 1-D velocity model (Arvidsson & Ekström 1998). We tested other filter parameters and report results in Section 4.2.

The automatic inversion consists of two main steps. First, the entire data set is inverted for a fixed depth (18 km) to remove traces with a low signal-to-noise ratio (high normalized variance $\geq$0.8) and large re-alignment. From tests, we found that the choice of the fixed depth of 18 km or of a different depth has little effect on the remaining data set, and basically no effect on our results. The remaining traces are then inverted for several depths. The 50–100 s data have little depth resolution, because long-period surface-wave excitation functions have little depth variation. Thus, we apply a limited number of depth-steps with increasing step width (10, 14, 18, 25, 31, 42, 55, 75, 100, 125, 150, 175 and 200 km) to find the best-fitting depth. We use a minimum 10 per cent variance increase to

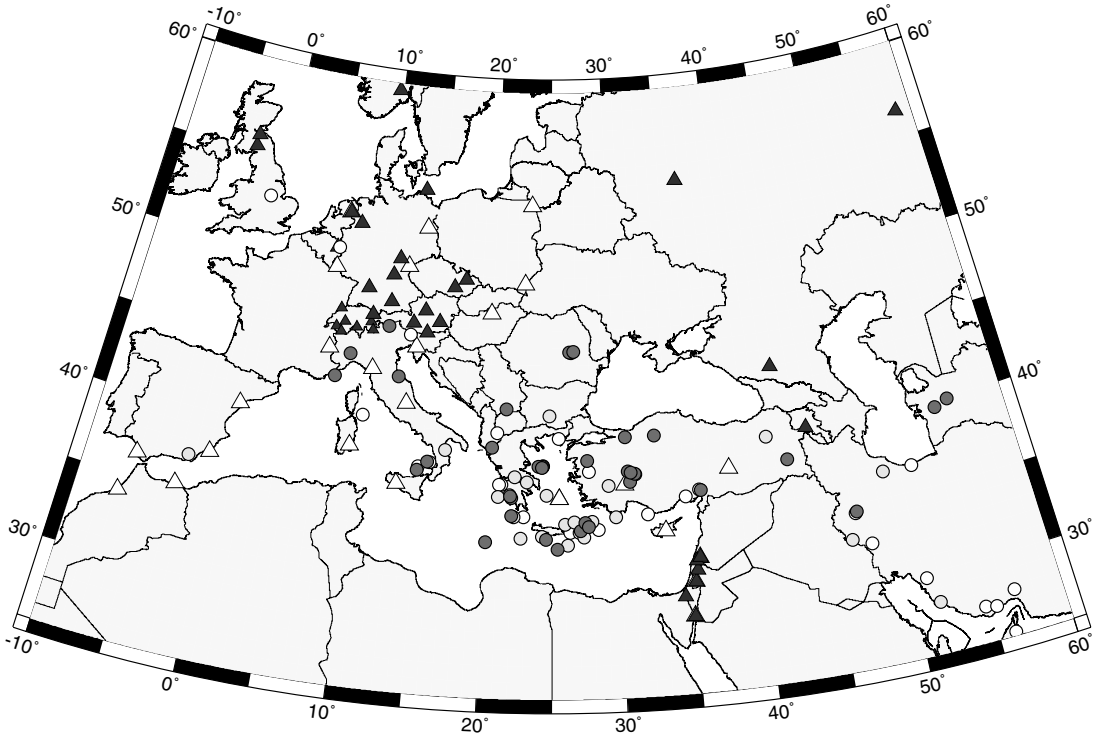

Figure 2. Map of near real-time accessible broad-band (BB) stations and automatic moment tensor solutions obtained between 2000 April and 2002 April (event Nr 37 in central Kazakhstan is not displayed). Solid triangles show stations available for this study. Open triangles depict stations that became available after 2002 April, but were not used here. We use only some of the 28 BB stations operated by the Swiss Seismological Service. No BB stations were available from the seismically active Aegean Sea region. Circles show the events analysed, and shading indicates the quality of the moment tensor solution (see Section 3.1): dark grey circles are *true* A-quality; light grey circles *true* B-quality; and open circles *true* C-quality solutions.

estimate depth uncertainty; our uncertainty range is simply defined by the trial depths that just exceed the 10 per cent increase. We consider this uncertainty estimate conservative, since the waveform fit degrades visibly.

3 QUALITY ASSESSMENT OF RESULTS

We started our procedure for automatic moment tensor inversion in 2000 April. By 2002 April, we had obtained 87 moment tensor solutions (Fig. 2, Table 1), mainly for events in the seismically active central-eastern Mediterranean region (Jackson & McKenzie 1988).

We check the quality of the automatic moment tensors because solution accuracy depends on event location, location precision, station distribution and signal strength. First, we use an independent high-quality moment tensor catalogue to quantify *true* quality. Second, in order to estimate solution quality automatically, we derive rules from solution parameters that reproduce overall *true* quality. We disseminate only the solutions that pass the automatically applied rules.

3.1 *True* quality

The Swiss automatic moment tensor (SAMT) catalogue contains many moderate events not included in global catalogues, which are incomplete below $M_w = 5.5$ and with very few $M_w \leq 5.0$ events. Therefore, we compared our automatic solutions with those of the Swiss Seismological Service's regional moment tensor (SRMT) catalogue. The SRMT catalogue covers the European-Mediterranean area and is nearly complete down to $m_b = 4.5$ (Braunmiller *et al.* 2002). SRMT solutions are derived with a more complete data set, available weeks to months after an event, than the data set used for SAMT analysis. SRMT solution quality is high based on comparison with other independent source parameter estimates available for selected events (Braunmiller *et al.* 2002). For a few events east of SRMT coverage (>55°E), we compared our solutions with the Harvard catalogue, or, when not available, with magnitudes given by the USGS.

The *true* quality of a SAMT solution is estimated by comparing its focal mechanism, depth and M_w with the SRMT solution. We distinguish three quality levels: A has well-resolved mechanisms, depths and M_w; B has only well-resolved M_w; and C is unreliable. Fig. 3 provides a sketch of the quality criteria described below.

The most stable focal mechanism parameters are the double-couple part and the orientation of the principal axes. Moment tensor solutions for a given earthquake included in different catalogues may show differences in the non-double-couple part ϵ [ratio of smallest to largest moment tensor eigenvalues, following Dziewonski *et al.* (1981)]. These differences are often introduced by an inaccurate source location (Zhang & Lay 1990), differences between the station configurations (Šílený & Vavryčuk 2002), inaccurate path models (Henry *et al.* 2002; Fröhlich 1994), or a poor resolution of $M_{r\phi}$ and $M_{r\theta}$ (Kuge & Lay 1994). We therefore use the mean difference of the axes $|\Delta Ax|$, defined as the average of the differences in the orientation of the principal axes, to estimate the similarity between SAMT and SRMT focal mechanisms.

The mean difference $|\Delta Ax|$ is zero for identical axes' orientations. Interchanging two axes (for example changing a normal to a thrust or a left-lateral to a right-lateral mechanism) results in $|\Delta Ax| = 60°$. We thus require A-quality solutions to have $|\Delta Ax| \leq 30°$;

Table 1. Table of the 87 automatic moment tensor solutions. From left to right: event number, PDE location, *true* and *assigned* quality, seismic moment M_o in N m, M_w, depth in km, orientation of the two nodal planes in degrees, number of stations and components used, quickly available location used for inversion. For completeness, we include all source parameters even for true B- and C-quality solutions. For B, only size is well resolved, and for C none of the parameters is reliably resolved. For further studies, use M_w, depth and focal mechanism from A, and only M_w from B solutions.

Nr	Location (PDE)				Quality		M_o	M_w	Depth	Plane 1			Plane 2			St.	Co.	Location used for inversion		
	Date	Time	Lat	Long	*True*	*Assigned*				Strike	Dip	Rake	Strike	Dip	Rake			Time	Lat	Long
1	00-04-06	00:10:38.0	45.72	26.58	A	A^a	.410E+17	5.01	125	0	20	58	213	72	101	27	50	00:10:39.0	45.70	26.60
2	00-04-21	12:23:10.0	37.83	29.31	B	B^a	.114E+18	5.31	31	336	49	−48	103	55	−127	11	13	12:23:05.0	36.80	29.40
3	00-05-24	05:40:37.7	36.04	22.01	A	A^a	.528E+18	5.75	25	269	47	4	176	86	137	20	44	05:40:35.7	36.10	21.90
4	00-06-06	02:41:49.8	40.69	32.99	A	A^a	.128E+19	6.01	10	8	43	−31	122	68	−128	26	66	02:41:56.7	41.30	32.90
5	00-06-13	01:43:14.0	35.15	27.13	A	A^a	.126E+18	5.34	18	227	82	1	137	88	172	28	74	01:43:18.0	35.30	27.20
6	00-06-15	21:30:29.0	34.44	20.18	A	B^a	.352E+17	4.97	42	40	45	65	253	49	112	10	16	21:30:34.4	34.50	20.00
7	00-07-25	19:33:56.0	37.13	21.99	A	A^a	.442E+17	5.03	42	333	36	−62	119	57	−109	25	41	19:33:47.7	37.50	24.00
8	00-08-21	17:14:26.0	44.87	8.48	A	A^a	.281E+17	4.90	10	114	34	−113	322	59	−74	30	65	17:14:26.0	44.80	8.60
9	00-08-23	13:41:28.0	40.68	30.72	A	A^a	.187E+18	5.45	31	251	71	−168	157	78	−18	29	77	13:41:26.0	40.40	30.70
10	00-11-15	15:05:37.0	38.35	42.93	A	A^a	.288E+18	5.58	18	217	20	37	92	77	106	5	10	15:05:24.7	38.40	44.00
11	00-12-06	17:11:06.4	39.57	54.80	A	A^a	.307E+20	6.93	42	110	44	80	302	46	98	6	18	17:11:07.9	39.70	54.90
12	00-12-15	16:44:47.6	38.45	31.35	A	A^a	.193E+19	6.13	18	290	30	−96	117	59	−86	25	62	16:44:45.0	38.60	31.10
13	01-02-25	18:34:42.2	43.46	7.47	A	A^a	.997E+16	4.60	31	249	22	93	65	67	88	16	24	18:34:32.6	42.90	7.40
14	01-03-10	11:20:57.8	35.08	26.37	C	B^a	.640E+17	5.14	75	146	46	110	297	47	69	11	23	11:20:59.3	35.60	27.00
15	01-03-23	05:24:12.2	32.92	46.65	B	C^a	.274E+18	5.56	18	307	16	22	196	84	104	3	6	05:24:21.8	33.60	45.30
16	01-03-28	16:34:21.8	29.69	51.18	C	C^a	.205E+17	4.81	18	313	43	54	178	55	119	5	5	16:34:22.0	29.80	51.20
17	01-03-30	15:30:49.0	38.01	30.94	A	A^a	.115E+17	4.64	25	44	29	−103	239	61	−82	15	24	15:30:53.0	38.70	30.80
18	01-04-03	17:36:34.1	32.45	47.99	C	C^a	.400E+17	5.01	18	106	38	−139	342	66	−59	4	6	17:37:27.0	31.50	49.80
19	01-04-08	06:12:27.8	38.38	22.18	B	B^a	.152E+17	4.73	175	337	41	74	177	50	103	15	18	06:12:27.0	38.30	22.30
20	01-04-09	17:38:39.2	40.11	20.37	A	A^a	.307E+17	4.93	31	294	68	22	195	69	156	18	35	17:38:51.0	39.80	20.40
21	01-04-10	14:00:07.6	34.30	26.17	B	B^a	.214E+17	4.82	42	4	46	−164	263	78	−44	12	14	14:00:11.0	34.30	26.10
22	01-05-01	06:00:54.1	35.64	27.49	A	B^a	.684E+17	5.16	10	337	37	−126	199	60	−65	12	35	06:00:55.0	35.80	27.40
23	01-05-04	19:52:01.9	34.72	22.74	B	C^a	.272E+17	4.89	10	13	25	28	256	78	112	2	3	19:52:32.0	36.00	21.00
24	01-05-17	11:43:58.2	39.02	15.47	A	A^a	.359E+17	4.97	200	152	16	−149	33	81	−75	11	17	11:43:57.5	38.90	15.50
25	01-05-24	17:34:01.1	45.75	26.46	A	A^a	.741E+17	5.18	150	0	30	61	212	63	105	22	42	17:33:55.6	45.80	26.70
26	01-05-29	04:43:56.4	35.39	27.75	A	B^a	.655E+17	5.15	25	314	65	−179	224	89	−24	12	27	04:43:56.0	35.40	27.70
27	01-06-10	01:52:08.0	39.87	55.89	A	C^a	.132E+18	5.35	25	114	34	57	331	61	110	2	2	01:52:11.8	40.50	53.60
28	01-06-22	11:54:48.5	39.35	27.34	A	A^a	.983E+17	5.27	25	353	52	−17	94	76	−141	15	28	11:54:48.0	39.40	27.70
29	01-06-23	06:52:41.9	35.71	28.02	B	B^a	.558E+18	5.77	31	239	53	−24	345	70	−140	10	23	06:52:45.4	35.80	28.10
30	01-06-25	13:28:46.4	37.20	36.17	A	A^a	.199E+18	5.47	10	346	19	−131	210	75	−76	10	25	13:28:49.8	37.10	35.90
31	01-07-10	21:42:06.4	39.88	41.59	B	C^a	.994E+17	5.27	31	284	71	−170	191	81	−18	4	6	21:41:49.9	39.20	44.30
32	01-07-17	15:06:15.6	46.74	11.37	A	A^a	.156E+17	4.73	10	208	40	−5	302	86	−130	10	16	15:06:16.3	47.00	11.50
33	01-07-20	05:09:39.2	45.77	26.78	A	A^a	.433E+17	5.03	100	281	12	20	171	85	101	10	25	05:09:10.0	44.00	29.00
34	01-07-26	00:21:37.0	39.06	24.34	A	A^a	.851E+19	6.56	25	231	67	−178	140	88	−22	24	70	00:21:37.5	39.10	24.30
35	01-07-26	04:53:34.0	39.02	24.28	A	A^a	.267E+17	4.89	31	243	58	176	335	87	31	13	21	04:53:33.1	39.10	24.30
36	01-07-30	15:24:57.0	39.04	24.01	A	A^a	.478E+17	5.06	18	227	64	−177	136	88	−25	23	56	15:25:06.0	39.70	23.90
37	01-08-22	15:58:01.2	47.24	70.04	A	A^a	.932E+17	5.25	18	149	57	172	243	83	32	3	9	15:58:10.1	47.70	69.30
38	01-09-13	15:42:52.2	35.54	25.97	B	B^a	.146E+17	4.71	42	227	44	−7	322	84	−133	12	18	15:42:59.6	34.90	26.90
39	01-09-16	02:00:47.3	37.24	21.88	A	A^a	.282E+18	5.57	10	118	46	−129	348	55	−56	17	43	02:00:48.4	37.40	22.00
40	01-09-25	11:53:32.4	36.01	32.13	C	C^a	.461E+18	5.71	42	106	87	178	196	88	2	1	2	11:53:36.1	35.90	32.30
41	01-09-26	04:19:56.3	35.04	27.04	C	B^a	.460E+17	5.05	10	306	7	68	147	83	92	7	12	04:19:08.6	31.60	30.20
42	01-10-15	08:51:09.9	35.99	22.18	B	B^a	.145E+17	4.71	125	332	65	−163	235	75	−25	10	13	08:50:44.4	34.80	23.60

Table 1. *(Continued.)*

Nr	Location (PDE)				Quality		M_o	M_w	Depth	Plane 1			Plane 2			St.	Co.	Location used for inversion		
	Date	Time	Lat	Long	*True*	*Assigned*				Strike	Dip	Rake	Strike	Dip	Rake			Time	Lat	Long
43	01-10-18	15:50:30.9	36.90	35.04	C	B^a	.206E+17	4.81	42	164	42	−45	291	61	−123	11	15	15:50:29.0	38.00	37.00
44	01-10-18	18:08:33.9	38.70	14.81	C	C^a	.345E+17	4.96	175	89	63	154	191	67	28	2	2	18:07:23.3	34.80	18.70
45	01-10-26	13:32:48.2	38.10	23.11	B	B^a	.168E+17	4.75	18	224	41	−168	126	82	−48	11	19	13:32:38.2	37.80	24.20
46	01-10-28	16:25:21.5	52.72	0.93	C	C^a	.415E+17	5.02	100	231	27	0	141	89	117	1	1	16:25:25.9	52.80	359.40
47	01-10-29	20:34:24.7	38.95	24.25	A	A^a	.321E+17	4.94	14	249	38	−138	124	65	−59	14	32	20:21:32.7	38.60	25.60
48	01-10-30	21:00:05.9	35.94	29.78	B	B^a	.632E+17	5.14	75	302	69	−165	207	76	−21	14	32	20:59:56.9	35.70	30.60
49	01-10-31	12:33:56.4	37.26	36.05	C	C^a	.149E+18	5.38	31	336	42	−134	209	60	−56	5	7	12:33:59.3	37.70	36.30
50	01-11-02	22:05:30.9	27.18	54.62	C	C^a	.336E+17	4.95	125	9	16	−46	145	78	−101	1	1	22:05:29.1	27.00	54.60
51	01-11-04	17:23:29.8	34.06	25.43	A	B^a	.203E+17	4.81	25	264	17	62	112	74	98	4	9	17:23:27.7	34.00	25.00
52	01-11-07	09:40:43.5	41.39	10.11	C	C^a	.296E+17	4.92	25	11	41	59	228	55	113	3	3	09:40:53.5	41.90	10.10
53	01-11-18	01:01:35.8	35.22	28.44	C	C^a	.232E+17	4.85	100	44	42	−114	255	52	−69	1	1	01:00:42.9	31.80	33.50
54	01-11-26	00:56:57.0	43.89	12.57	A	A^a	.129E+17	4.68	18	8	53	−43	127	56	−134	6	12	00:57:01.0	43.60	12.50
55	01-11-26	05:03:20.9	34.83	24.28	B	B^a	.615E+17	5.13	14	133	21	115	286	70	80	13	25	05:03:08.6	34.50	25.60
56	01-12-10	19:50:08.6	37.30	24.62	B	C^a	.120E+17	4.66	31	38	37	70	242	54	104	1	1	19:50:04.4	37.20	25.00
57	01-12-11	16:34:05.1	39.01	24.28	C	C^a	.130E+17	4.68	150	159	31	80	350	58	95	3	3	16:33:22.5	38.30	28.00
58	01-12-30	04:06:28.0	34.78	27.38	B	B^a	.108E+18	5.29	100	238	29	−33	357	74	−115	8	9	04:06:58.5	35.70	25.00
59	02-01-01	22:15:57.7	37.29	21.83	C	C^a	.248E+17	4.87	175	272	12	−132	135	81	−81	2	2	22:15:06.7	35.50	26.00
60	02-01-09	09:35:56.2	37.90	21.22	C	C^a	.414E+17	5.01	31	206	36	−109	50	56	−76	1	2	09:35:23.4	36.60	23.70
61	02-01-09	14:11:08.0	35.99	22.91	C	C^a	.357E+17	4.97	10	122	15	−119	332	76	−82	4	4	14:10:26.5	34.20	25.80
62	02-01-21	14:34:23.8	38.68	27.82	C	C^a	.175E+18	5.43	10	259	69	0	349	89	−159	2	4	14:33:10.7	35.20	35.60
63	02-01-22	04:53:52.2	35.68	26.68	B	B^a	.257E+19	6.21	42	55	20	−118	265	72	−79	15	36	04:53:53.7	35.70	26.70
64	02-01-26	20:05:35.9	37.16	20.98	B	B^a	.648E+17	5.14	18	314	22	25	200	80	110	8	17	20:05:11.5	36.30	23.00
65	02-02-03	07:11:28.8	38.49	31.31	A	A^a	.797E+19	6.54	14	241	37	−122	100	59	−67	20	59	07:11:36.1	38.80	31.20
66	02-02-03	09:26:43.6	38.63	30.81	A	A^a	.904E+18	5.91	25	231	42	−51	4	58	−119	21	55	09:26:43.2	38.60	30.90
67	02-02-03	11:54:34.6	38.56	31.03	A	A^a	.104E+18	5.28	18	275	42	−61	58	53	−113	10	20	11:54:36.3	38.50	31.20
68	02-02-04	20:09:32.1	37.14	357.57	B	A^a	.429E+17	5.03	10	190	19	−11	291	85	−109	17	29	20:09:32.4	37.30	357.30
69	02-02-14	03:18:01.7	46.37	13.23	C	C^a	.358E+15	3.64	200	316	41	−112	165	52	−71	1	2	03:18:01.0	46.40	13.40
70	02-02-17	13:03:52.9	28.12	51.75	B	B^a	.955E+17	5.26	55	344	56	−167	247	79	−34	7	9	13:03:52.7	28.10	51.90
71	02-03-05	05:23:45.8	40.67	25.57	C	C^a	.144E+17	4.71	42	85	80	0	355	89	170	4	4	05:23:48.3	40.80	25.20
72	02-03-07	20:30:40.1	40.98	20.77	C	C^a	.653E+17	5.15	125	195	13	63	43	78	95	1	1	20:29:01.5	39.60	30.10
73	02-03-10	12:39:38.3	39.01	15.65	C	C^a	.509E+17	5.07	42	129	4	−177	37	89	−85	1	1	12:40:34.0	42.50	13.10
74	02-03-11	20:06:37.1	25.23	56.13	C	C^a	.128E+18	5.34	42	172	48	−54	304	52	−123	2	3	20:06:31.8	24.50	57.70
75	02-03-17	14:46:27.8	50.77	6.17	C	C^a	.964E+16	4.59	75	154	54	−136	35	55	−44	1	1	14:46:27.0	51.10	6.00
76	02-04-04	15:44:31.9	27.01	55.34	C	C^a	.899E+16	4.57	55	155	45	−36	273	64	−129	1	1	15:44:31.0	27.00	55.30
77	02-04-05	04:52:23.5	38.48	14.74	A	A^a	.561E+16	4.44	14	40	50	44	278	57	130	6	12	04:52:22.0	38.40	15.10
78	02-04-05	07:55:48.6	37.92	21.03	C	C^a	.322E+18	5.61	200	72	20	117	223	72	80	1	2	07:55:32.9	37.40	22.60
79	02-04-05	13:14:02.0	42.02	24.83	B	B^a	.168E+17	4.75	10	194	20	179	285	89	69	8	13	13:14:01.0	42.10	24.80
80	02-04-08	18:31:05.2	36.56	52.01	C	C^a	.462E+17	5.05	18	97	30	55	316	65	108	3	4	18:31:0.0	36.50	52.20
81	02-04-15	08:10:06.1	34.66	24.59	A	B^a	.207E+17	4.81	10	23	8	177	116	89	81	8	12	08:10:06.9	34.90	24.20
82	02-04-17	06:42:53.1	39.79	16.77	B	A^a	.410E+17	5.01	14	142	13	55	357	78	97	19	39	06:42:53.0	39.80	16.80
83	02-04-17	08:47:22.7	27.72	56.81	C	C^a	.241E+18	5.53	25	304	17	−82	117	72	−92	1	2	08:47:23.8	27.90	56.80
84	02-04-19	13:46:49.6	36.57	49.85	B	C^a	.787E+17	5.20	18	185	26	115	337	66	77	4	7	13:46:49.0	36.60	49.90
85	02-04-24	10:51:50.9	42.41	21.42	A	A^a	.474E+18	5.72	14	245	35	−84	58	54	−93	22	61	10:51:51.5	42.40	21.40
86	02-04-24	19:48:07.0	34.54	47.33	A	A^a	.172E+18	5.43	14	314	65	−177	223	87	−24	6	14	19:48:07.0	34.50	47.30
87	02-04-24	20:11:21.5	34.43	47.23	C	C^a	.888E+17	5.24	25	32	74	−4	124	85	−164	3	3	20:11:08.6	37.30	38.10

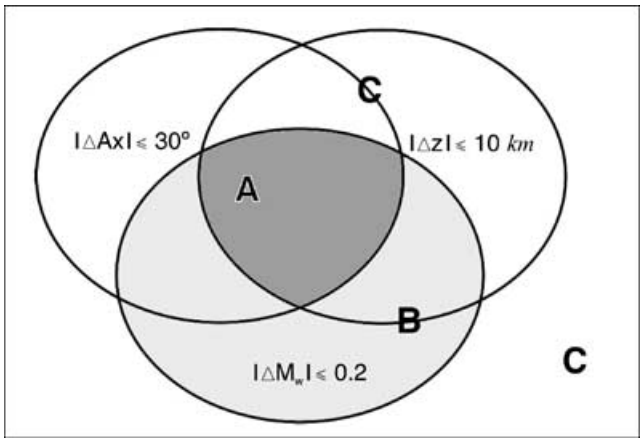

Figure 3. Sketch of *true* quality assignment. The *true* quality of each automatic solution is based on the orientation of the mean principal axes $|\Delta\mathbf{Ax}|$, depth $|\Delta\mathbf{z}|$ and magnitude $|\Delta M_w|$ differences relative to SRMT solutions (see text for details). Dark grey shaded area corresponds to *true* quality A, light grey to *true* quality B, and white to *true* quality C.

solutions with $|\Delta Ax| > 30^\circ$ are either B or C quality, depending on the magnitude difference (Fig. 3). Fig. 4 (top) shows the distribution of $|\Delta Ax|$. For A-quality solutions, the mean value of $|\Delta Ax|$ is 18.8° ± 6.7°. Two of the solutions with $|\Delta Ax| \leq 30^\circ$ are not A quality, because one violates the depth criterion (B quality) and one the magnitude criterion (C quality).

We also checked the focal parameter agreement between the SAMT and SRMT catalogues using the radiation pattern coefficient η_P (Kuge & Kawakatsu 1993), a parameter describing the radiation pattern similarity of two mechanisms. Our median $\eta_P = 0.85$ for A-quality solutions compares well with the median of $\eta_P = 0.88$ found by Helffrich (1997), who compared ERI, Harvard and USGS catalogues for shallow earthquakes (most SAMTs are for shallow earthquakes).

Because of the low-depth resolution and the discrete set of trial depths, we require that the difference $|\Delta z|$ between the SAMT depth range (best-fitting depth plus uncertainty) and the SRMT depth is ≤10 km for an A-quality solution. A similar scheme was proposed by Kubo *et al.* (2002) when comparing the Japanese regional NIED catalogue with the Harvard-CMT and the Japanese Meteorological Agency (JMA) focal mechanism catalogues. Differences $|\Delta z| > 10$ km result in B or C solutions (Fig. 3). Fig. 4 (middle) shows $|\Delta z|$ for the three quality groups.

The difference between SAMT and SRMT M_w estimates must be ≤0.2 units for an A- or B-quality solution [$M_w = (\log M_o/1.5) - 10.73$, following Kanamori (1977)]. A required difference $|\Delta M_w| \leq 0.2$ is consistent with Pasyanos *et al.* (1996), who found that automatic and revised regional MT solutions in northern California have M_w estimates that usually differ by less than 0.2 units, even when the focal mechanism and depth estimates differ strongly. M_w depends mainly on the signal amplitude and is therefore the parameter easiest to resolve. One goal for our automatic procedure is to provide robust M_w values so that disaster relief agencies may quickly estimate possible earthquake damage. Damage is governed by the rupture process and local site effects; our M_w can only help to estimate whether no, local or widespread damage is to be expected. Therefore we accept an M_w estimate as accurate even when the focal mechanism and/or the depth exceed their A-quality threshold: these are our B-quality solutions. $|\Delta M_w| > 0.2$ are C quality, irrespective

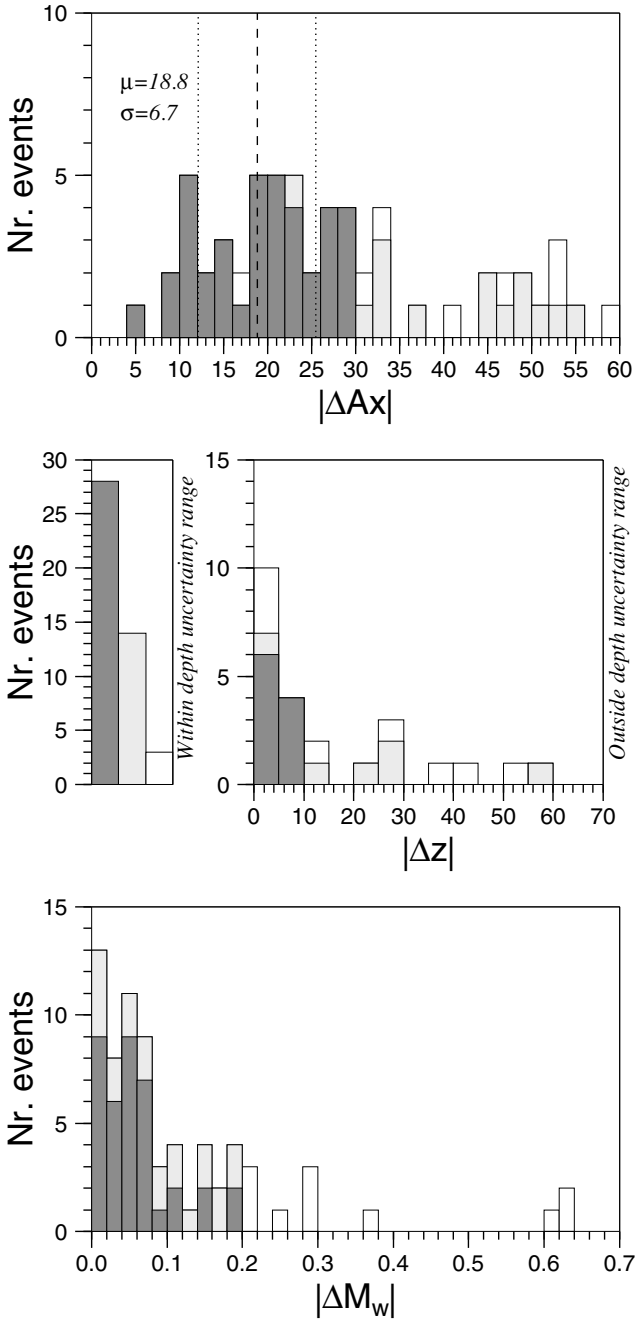

Figure 4. Top: mean principal axes' orientation difference $|\Delta Ax|$ relative to SRMT for *true* quality A, B and C. Middle: depth difference $|\Delta z|$ relative to SRMT. Solutions are divided into two panels: left panel shows the number of quality A, B and C solutions where the SAMT depth uncertainty range includes the SRMT depth. Right panel shows $|\Delta\mathbf{z}|$ for SRMT depth estimates outside the SAMT depth uncertainty range. Bottom: $|\Delta M_w|$ relative to SRMT. Not all B and C solutions are shown in each panel. See text for details. Colour scale as in Fig. 2.

of focal mechanism and depth (Fig. 3). The distribution of $|\Delta M_w|$ is shown in Fig. 4 (bottom).

For our data we observe that SAMTs with $|\Delta Ax| \leq 30^\circ$ usually have $|\Delta z| \leq 10$ km and $|\Delta M_w| \leq 0.2$. Based on our rules, the 87 automatic moment tensors are divided into 38 A-quality, 21 B-quality and 28 C-quality solutions.

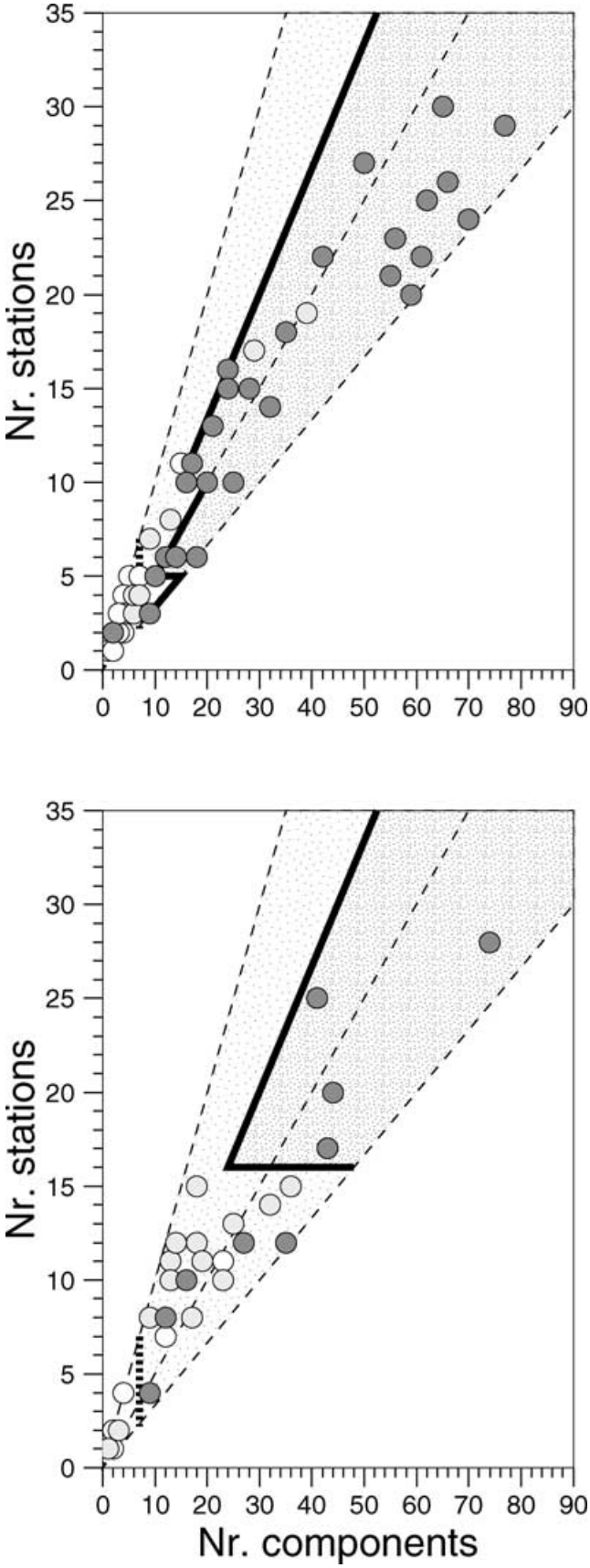

Figure 5. Empirical rules to assess *assigned* quality are based on the number of stations and components used to obtain the MT solutions. Dark grey circles are *true* quality A, light grey circles are B, and open circles are C solutions. On and right of the black thick line is *assigned* quality A^a (densely stippled area); the lightly stippled area marks *assigned* B^a; on and left of the vertical thick dashed line are C^a solutions (numerical values are given in Table 2). Thin dashed lines (from left to right) indicate one, two or three components used for each station. The top plot is for the entire European-Mediterranean area; the bottom plot is for events in the southern Aegean Sea, where we generally need data from more stations to obtain *true* A quality, because of long average station–event distances.

Table 2. Empirical rules applied to derive the *assigned* quality. The number of stations (*St*) and components (*Co*) used characterize the solution quality (Fig. 5). Rules for earthquakes located in the southern Aegean Sea ($34^\circ \leq$ Lat $\leq 38.5^\circ$; $20^\circ \leq$ Long $\leq 30^\circ$) are slightly different (right): there, a larger number of stations is required to obtain *assigned* quality A.

Quality	Rules (Europe-Mediterranean)	Rules (Southern Aegean Sea)
A	$St \geq 10$ & $Co/St \geq 1.5$ $St \geq 5$ & $Co/St \geq 2$ $St \geq 3$ & $Co/St = 3$	$St \geq 16$ & $Co/St \geq 1.5$
B	All other solutions	All other solutions
C	$Co \leq 7$	$Co \leq 7$

3.2 *Automatic assigned* quality

The *true* quality can be verified only *a posteriori*. For automatic solution dissemination, we derive empirical rules, matching the *a posteriori true* qualities that can be implemented into the automatic procedure. The rules are based on three principles.

(1) Applied to the whole data set, the rules should closely follow the *true* quality.

(2) The rules should not overestimate quality: *true* B-quality solutions should not be *assigned* A^a, and C-quality solutions should not be *assigned* A^a or B^a (we use the superscript 'a' to denote *assigned* quality). We want to have high confidence that an automatic A^a solution is truly A.

(3) The rules should be simple.

A combination of the number of stations and components used (i.e. seismograms with good signal-to-noise ratio) provides a simple yet reasonably accurate measure to assess solution quality (Table 2). The empirical rules were defined based on the 2000 April to 2002 April data set and may be modified when, for example, station availability increases. Fig. 5 shows that it is generally sufficient to use two or more components for each station to obtain A-quality solutions, even when only a few stations can be used. Using fewer stations and components results in lower-quality solutions. Many solutions of earthquakes located in the larger Iran area result in quality B or C, because of the low number of stations available. For the southern Aegean Sea ($34^\circ \leq$ Lat. $\leq 38.5^\circ$; $20^\circ \leq$ Long. $\leq 30^\circ$) we observe an interesting difference: we need more stations and components to obtain *true* A-quality solutions (Fig. 5). This exception is possibly due to large event–station distances (Fig. 2).

The empirical rules were designed to not overestimate *true* quality. Underestimating a few events is implicitly allowed, and results in fewer *assigned* A^a- and B^a-quality solutions compared with *true* quality. Undesired upgrade happens for only two events from B to A^a (6 per cent of the 34 *assigned* A^a-quality solutions) and for three

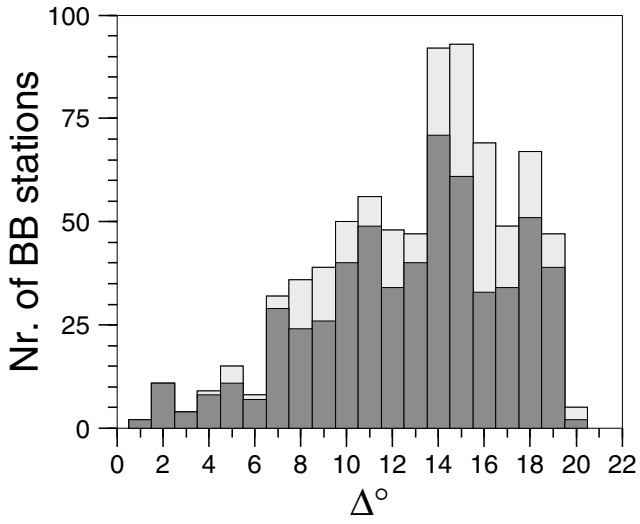

Figure 6. Cumulative number of stations used to obtain all A-quality (black) and B-quality (grey) solutions versus distance from epicentre. Most BB stations are located in areas of low seismicity (Fig. 2), resulting in large event–station distances. Obtaining more high-quality solutions or successfully analysing smaller events in the future depends critically on the improved availability of nearby ($\Delta \leq 7^\circ$) stations.

events from C to B^a (14 per cent of the 22 *assigned* B^a-quality solutions). No *true* C event is assigned to A^a. Such upgrades are confined to smaller events ($M_w \leq 5.3$). The empirical rules actually reproduce 82 per cent of the *true* quality data set; most differences (11 events) are caused by quality downgrade. Based on these observations, we have high confidence that our automatically disseminated solutions cause few (or no) false alerts for large, potentially damaging earthquakes.

4 DISCUSSION

4.1 Performance

In this section we focus on the geographical event distribution and factors that cause *true* low-quality solutions. We also compare our M_w, depth and focal mechanism results with the SRMT, the Harvard (CMT) and INGV (MEDNET) moment tensor results to illustrate their high consistency.

The distribution of the analysed events (circles, Fig. 2) reflects long-term seismicity (Jackson & McKenzie 1988). The distribution of high-quality solutions, however, is also affected by the station distribution (black triangles, Fig. 2). Generally, analysis is hampered by long average event–station distances (Fig. 6). Most data come from stations at distances $\Delta > 7^\circ$ with a peak around $\Delta = 14^\circ$–15° caused by high seismicity in the Aegean Sea and high station density in central Europe. Most high-quality solutions are produced for earthquakes in the central-eastern Mediterranean region, where data from stations in central Europe, Israel, the Caucasus region and Russia provide good azimuthal coverage. In the western Mediterranean region, seismicity is relatively low and the inadequate station distribution resulted in a B-quality solution for the one event analysed. Station coverage for events in the Caspian Sea and Zagros mountain regions is also low, and few of the frequent events have well-recovered source parameters. In central and northern Europe we obtained few high-quality automatic solutions. Although a large number of stations are available, the low-pass filter at 50 s precludes moment tensor retrieval for the typically smaller ($M_w < 4.5$) events of this region.

Not all events triggered by our automatic procedure resulted in a moment tensor. Triggered events result in *no solution* when either (1) no data are available, (2) the automatic alert is a false alarm, (3) the epicentre is strongly mislocated, (4) the true magnitude is far lower than the alert magnitude, or when any of these cases combine. Case (4) caused most *no-solution* events due to the low trigger threshold set for analysis ($M \geq 4.7$), which ensures the processing of all stronger events. We let the procedure decide whether a solution can be produced or not. For a few smaller events, few traces containing only long-period noise were inverted, resulting in C-quality solutions.

Earthquake size is the most stable source parameter and a few, good signal-to-noise seismograms generally constrain the seismic moment M_o. Fig. 7 shows the high correlation of the automatic M_w estimates relative to M_w from SRMT, CMT and MEDNET . Mean differences are very small, $\mu \leq 0.02$ relative to SRMT and CMT, and lower than 0.1 unit relative to MEDNET, with standard deviations close to 0.1. The linear regressions (dashed lines in Fig. 7) have slopes close to 1 and small intercepts, roughly consistent with a one-to-one relation between the magnitude estimates. We did not interpret small apparent differences because the data set is too small. Mean differences and regressions were determined for A- and B-quality solutions combined, because we did not see any significant systematic difference in the A- and B-quality M_w estimates (Fig. 4, bottom).

A-quality solutions were obtained for earthquakes from $M_w = 4.5$ to $M_w = 7.0$. In general, larger events ($M_w \geq 5.5$) result in A-quality solutions (Fig. 8), and earthquakes with $M_w \leq 5.5$ result in quality A or B. We obtained three B-quality solutions for earthquakes with $M_w \geq 5.5$; in all cases, the lower quality was caused by the inaccurate quick location used for the inversion. We repeated the inversion with the PDE location. In two cases we obtained A-quality solutions. One case remained B quality, because of $|\Delta Ax| = 31^\circ$, just outside the A-quality criterion ($|\Delta Ax| \leq 30^\circ$); the depth and magnitude differences both satisfied the A-quality criteria. The number of MT solutions and the ratio of A/B solutions decrease for earthquakes with $M_w \leq 5.0$ due to lower signal strength and the large event–station distances (Fig. 6).

Fig. 9 illustrates the limitations of long-period ($T \geq 50$ s) analysis with respect to magnitude or signal strength. Variance increases with decreasing event size, effectively setting the lower limit for retrieving MT solutions to $M_w \approx 4.5$. At such long periods signal strength at smaller magnitudes is just slightly above the noise level. We also observe that the variance for B-quality solutions is higher than it is for A-quality solutions.

Long-period surface waves offer only limited depth resolution (Giardini 1992). However, the depths of A-quality solutions agree very well with those in SRMT, CMT and MEDNET (Fig. 10). The mean difference μ is always ≤ 4 km with a standard deviation of $\sigma \leq 15$ km. Our SAMT catalogue contains only three deep earthquakes with quality A, and we observe no significantly greater depth estimate differences for these events. Events with a large depth difference ($|\Delta \mathbf{z}| \geq 20$) are different events in each panel, reflecting the depth differences in the catalogues used for comparison. Note that A-quality solutions for shallow and deep earthquakes are always correctly distinguished.

Fig. 11 shows the focal mechanisms of the *true* A-quality solutions together with the available SRMT, CMT and MEDNET solutions. Focal mechanisms show excellent agreement for all earthquakes: shallow, deep, weak and strong. Larger differences exist for

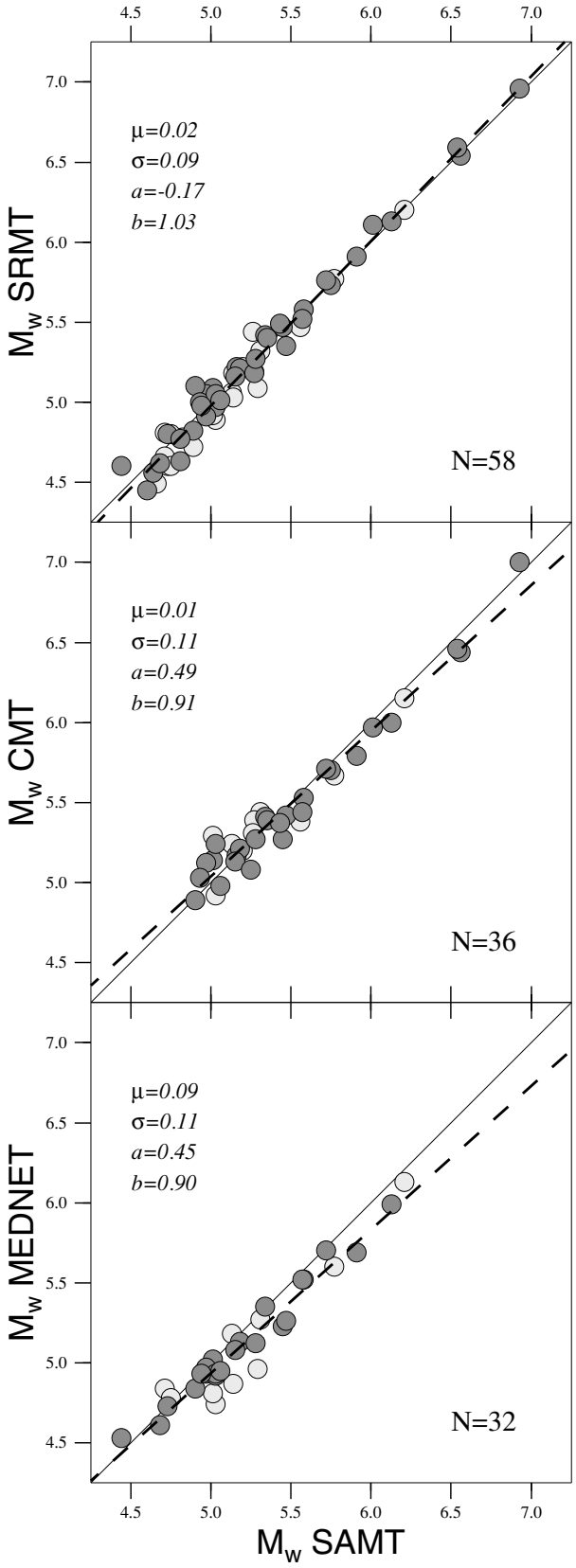

Figure 7. Automatic M_w estimates relative to SRMT (top), CMT (middle) and MEDNET (bottom). Mean difference (μ), standard deviation (σ), slope and intercept of the linear regression ($y = a + bx$, dashed line) are computed for qualities A and B combined. The solid line represents a one-to-one relation. Colour scale as in Fig. 2.

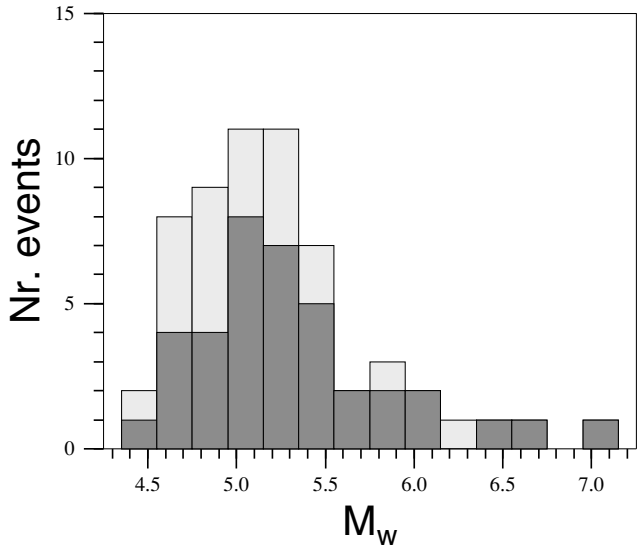

Figure 8. Number of *true* quality A and B solutions relative to SRMT M_w estimates. Colour scale as in Fig. 2.

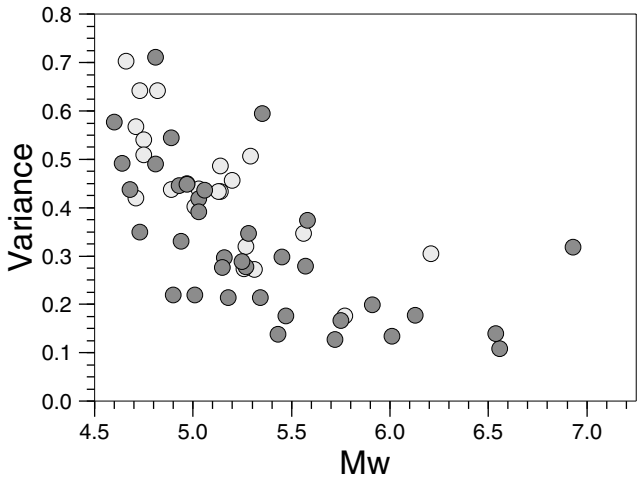

Figure 9. Correlation between normalized variance and M_w for solutions of *true* quality A and B. Colour scale as in Fig. 2.

only three CMT solutions (Nr. 20, 33, 36). These earthquakes are small ($M_w = 5.0-5.1$) for CMT analysis. Their CMTs have large non-double-couple parts ϵ ($0.316 \leq \epsilon \leq 0.342$) and large relative moment tensor uncertainties E ($0.261 \leq E \leq 0.673$), compared with the average values $\overline{\epsilon} = 0.124$ and $\overline{E} = 0.165$ of all 19 589 CMT solutions (1976 until 2002 November). E is defined in Davis & Fröhlich (1995). Moment tensors with high ϵ and E have poorly constrained focal parameters (Fröhlich *et al.* 1997).

4.2 Frequency band and location

Our goal is to retrieve as many A-quality solutions as possible, even for smaller earthquakes ($4.5 \leq M_w \leq 5.0$), while minimizing the number of C-quality solutions. Solution quality depends on station distribution, location accuracy and the ability to match phases correctly in the seismograms. For the given station distribution (Fig. 2), we performed two tests. First, we tried to find the optimum frequency band for analysis with the quickly available locations and data set

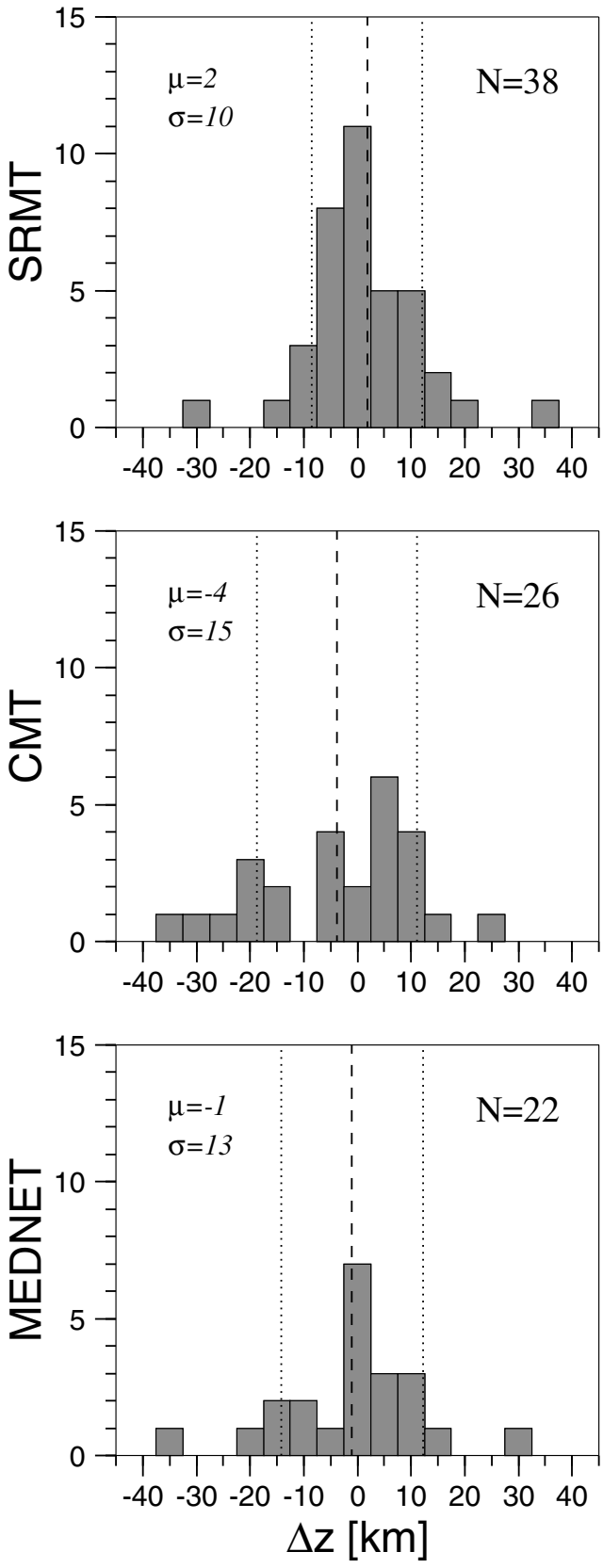

Figure 10. SAMT depth estimate differences for *true* A-quality solutions relative to SRMT (top), CMT (middle) and MEDNET (bottom). Differences are small: mean differences (long dashes) are $\mu \leq 4$ km with standard deviations (short dashes) $\sigma \leq 15$ km.

used for near real-time processing. The frequency band needs to match phases, which is easier at longer periods, and have good signal-to-noise ratio, which is higher at shorter periods. We thus performed inversions for five selected period ranges (40–60, 45–80, 50–100, 60–125, and 70–140 s). In a second step, we repeated the same analysis with the more accurate PDE locations to see whether location accuracy affects the choice of frequency band.

The number of quality A, B and C solutions is strongly dependent on frequency band (Fig. 12, top left). The largest number of A-quality solutions (and highest ratio of A/C solutions) is obtained with the 50–100 s band for the quickly available locations. Using the more accurate PDE locations, the optimal period range shifts to lower periods of 45–80 s (Fig. 12, bottom left). The reason for this shift is that mislocation introduces errors in the initial phase, which are then mapped onto the moment tensor. The effect is smaller at longer periods (Patton & Aki 1979), and the accuracy of the quick locations sets the optimum period range to 50–100 s. At longer periods (60–125, 70–140 s) the number of A- and B-quality solutions decreases for the quick and the PDE locations because of weak signals for the smaller events. At these period ranges, only stronger earthquakes can be analysed.

For shorter periods (40–60 s), the number of A-quality solutions decreases strongly even for the PDE locations. In most cases, A-quality solutions at 45–80 s (or 50–100 s) become B at 40–60 s (Fig. 12, bottom left). At periods below 50 s, surface waves become more sensitive to crustal thickness and average crustal velocity variations so that significant traveltime differences relative to PREM result (Larson & Ekström 2001; Pasyanos *et al.* 2001). Unresolved near-source earth structure may also cause surface-wave amplitude anomalies (van der Lee 1998). Both phase and amplitude differences limit reliable moment tensor retrieval below 50 s period for our uneven station distribution and our average event–station distances of about 1500 km.

The frequency band chosen has little effect on the overall quality of the focal mechanism and depth estimates for A-quality solutions. This also holds for the M_w estimates for A- and B-quality solutions measured relative to SRMT (Fig. 12). The median values of the radiation pattern coefficient η_P are generally high, close to the value found by Helffrich (1997), and decrease only slightly for shorter periods. There is no significant change for the mean depth difference; all means are $\mu < 3$ km with standard deviations $\sigma < 15$ km. Magnitude M_w differences for A- and B-quality solutions are close to 0.0 units with standard deviation $\sigma < 0.1$.

From our tests, we deduce that the 50–100 s period range is the best average range with the quickly available locations for the entire European-Mediterranean region. It allows routine MT analysis for earthquakes down to $M_w \approx 4.5$.

4.3 Current improvements

Two factors limit automatic retrieval of well-resolved MT for $M_w \geq 4.5$ earthquakes: location accuracy (Fig. 12), usually lower for smaller events ($M_w < 5.0$), and the limited, inhomogeneous distribution of near real-time accessible stations (Fig. 2).

Location accuracy is more important for shorter-period analysis. Accurate quick locations are starting to become routinely available from the European-Mediterranean Seismological Centre (EMSC). The EMSC merges automatic arrival-time picks from several European institutions, and the virtual network's improved station coverage and aperture is capable of accurate automatic locations (Bossu *et al.* 2002). The locations we have received since 2002 June are of good quality.

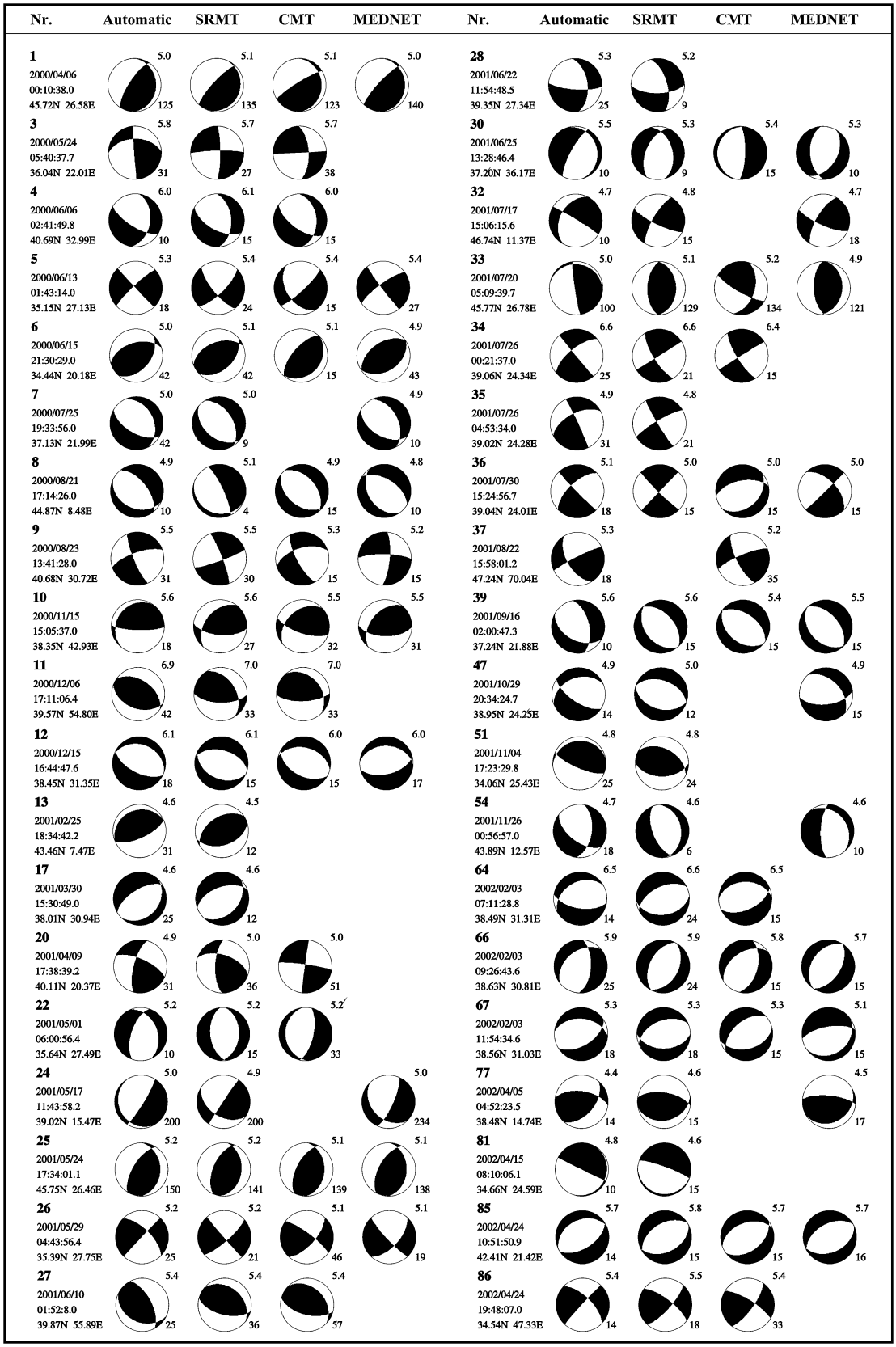

Figure 11. Focal mechanisms of the 38 *true* A-quality solutions (first column), compared with SRMT (second column), Harvard-CMT (third column) and MEDNET (fourth column) solutions. For each event, event number (Table 1), date and location (PDE) are given. Depth (km) and M_w are indicated on the bottom and top of each focal mechanism respectively. Focal mechanisms show a very good agreement. Automatic moment tensor inversion with complete regional seismograms in the period range of 50–100 s allows robust MT retrieval for earthquakes with $M_w \geq 4.5$. Large differences for three Harvard CMT solutions (Numbers 20, 33, 36) are discussed in Section 4.1.

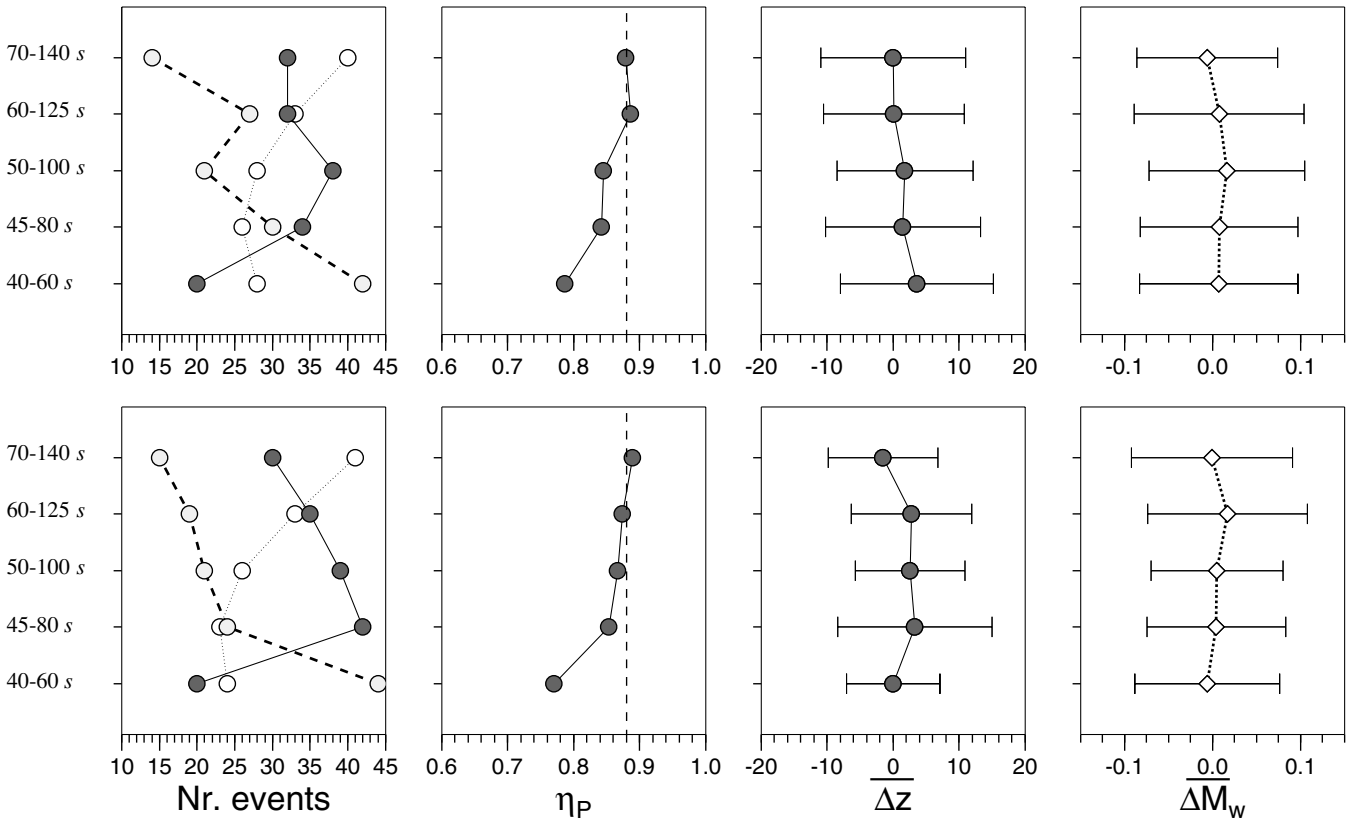

Figure 12. Performance of the automatic MT inversion routine for five period ranges with quickly available (top) and PDE (bottom) locations. From left to right. (1) Number of *true* quality A, B and C solutions. (2) Median values of the radiation pattern correlation coefficients η_P (quality A). The vertical dashed line is the median $\eta_P = 0.88$ obtained by Helffrich (1997) comparing ERI, Harvard and USGS catalogues. (3) Mean depth differences $\overline{\Delta \mathbf{z}}$ with error (quality A). (4) Mean M_w difference $\overline{\Delta M_w}$ with standard deviation (quality A and B combined). η_P, $\overline{\Delta \mathbf{z}}$ and $\overline{\Delta M_w}$ are relative to SRMT. Focal mechanism, depth and M_w estimates are well constrained for all period ranges, but performance changes: with quickly available locations, the best period range for our inversions is 50–100 s; with PDE locations it is 45–80 s. Colour scale as in Fig. 2.

The geographical distribution of near real-time accessible broad-band stations is limited and inhomogeneous (Fig. 2). In the context of the European MEREDIAN project (van Eck *et al.* 2001), the ORFEUS data centre now has near real-time access to an increased (and still growing) number of broad-band stations. Their distribution (white triangles, Fig. 2) partially fills gaps such as the western and central Mediterranean Sea, Turkey and eastern Europe. Northern Africa, however, lacks sufficient broad-band instruments. For events since mid-2002, these data are available to us. Preliminary scanning of the results shows that the smaller epicentral distances overall and improved azimuthal coverage increases the number of A-quality relative to B- and C-quality solutions.

Better quick locations and a denser network (and the resulting reduced epicentral distances) may also speed up analysis and lower magnitude thresholds in the future. For closer epicentral distances, 15-min seismograms contain the entire surface wave train. Reducing the seismogram length by 50 per cent and assuming faster data accessibility means that automatic solutions could be obtained within 45–60 min of an event. At closer epicentral distances, signal strength is greater and relatively less perturbed by crustal and upper-mantle heterogeneities. Combined with analysis at shorter periods, we would expect more reliable source parameter estimates for smaller events than is possible now.

Although improved EMSC locations and additional data from ORFEUS started becoming available in mid-2002, we have not included these more recent events here. We wanted to have constant conditions—location and data access—for the entire period covered in this paper and therefore did not mix the two intervals.

5 SUMMARY AND OUTLOOK

We have presented a fast and fully automatic procedure for moment tensor retrieval of moderate to strong ($M_w \geq 4.5$) earthquakes in the European-Mediterranean region using long-period (50–100 s) regional ($\Delta \leq 20^\circ$) seismograms. Automatic solutions are currently available within 90 min of an event. From 2000 April to 2002 April, we obtained 87 moment tensor solutions that we grouped into three qualities based on the similarity of the orientation of the main stress axes, depth and M_w with an independent, high-quality moment tensor catalogue. For 38 A-quality solutions, magnitude, depth and focal mechanisms are well-resolved; 21 B-quality solutions have well-resolved magnitude; and 28 C-quality solutions are not reliable. We derived simple empirical rules based on the number of stations and components used to predict the quality of a solution without a seismologist's interference. Automatic quality A^a MTs are disseminated to EMSC (*http://emsc-csem.org*), quality A^a and B^a solutions are displayed on our web page (*http://www.seismo.ethz.ch/mt*), A^a and B^a solutions can be obtained via e-mail (contact first author for details).

In the near future, we foresee highly improved near real-time automatic waveform analysis capabilities and successful routine MT applications to smaller earthquakes ($M_w \approx 4.0$) for most of the

European-Mediterranean region. Many national networks are making the transition to broad-band stations with near real-time data transmission. Connecting these national data centres via the internet will create a dense European-wide virtual network that could be used for near real-time event detection, size determination and MT inversion in the European-Mediterranean region. We can realize this scenario by increasing both the number of broad-band stations, particularly where no or few stations currently exist, and near real-time open access to these data for the scientific community.

ACKNOWLEDGMENTS

We thank Daniel Stich and an anonymous reviewer for their constructive comments. We thank Suzan van der Lee and Yuan Gao for providing modified moment tensor analysis codes. We appreciate discussions with Günter Bock about the topic—we will miss him. We thank Kathleen J. Jackson for enhancing the manuscript by correcting our grammar. Most figures were produced with GMT (Wessel & Smith 1995). High-quality near real-time broad-band data were obtained from the following institutions and networks: GEOFON, Potsdam (Germany); Gräfenberg Seismological Observatory, Erlangen (Germany); Institute of Physics of the Earth, Masaryk University, Brno (Czech Republic); MEDNET, Istituto Nazionale di Geofisica e Vulcanologia, Roma (Italy); National Data Centre, Soreq (Israel); Zentralanstalt für Meteorologie und Geodynamik, Wien (Austria); and the additional members of the MEREDIAN consortium and its lead agency ORFEUS, De Bilt (The Netherlands). Quick earthquake locations are send to us by EMSC (France); Geol. Survey B-W, Freiburg (Germany); GERESS array (Germany); GSR, Obninsk (Russia); IGN, Madrid (Spain); INGV, Rome (Italy); IPRG, Tel Aviv (Israel); LDG, Paris (France); NEIC (USGS); NIEP, Bucharest (Romania); SDAC, Hannover (Germany); (see *http://www.seismo.ethz.ch/redpuma*).

REFERENCES

Arvidsson, R. & Ekström, G., 1998. Global cmt analysis of moderate earthquakes, $mw \geq 4.5$, using intermediate-period surface waves, *Bull. seism. Soc. Am.,* **88,** 1003–1013.

Bossu, R., Mazet-Roux, G., Tome, M., Carreno, E., Guilbert, J., Menechal, Y., Schindele, F. & di Giovambattista, R., 2002. Emsc early warning system and real time seismicity, *EMSC Newsletter,* **18,** 2–5.

Braunmiller, J., 1998. Seismotectonics of the Explorer Region and of the Blanco Transform Fault Zone, *PhD thesis,* Oregon State University.

Braunmiller, J., Nábělek, J., Leitner, B. & Qamar, A., 1995. The 1993 klamath falls, Oregon earthquake sequence: source mechanisms from regional data, *Geophys. Res. Lett.,* **22,** 105–108.

Braunmiller, J., Kradolfer, U., Baer, M. & Giardini, D., 2000. Regional moment-tensor inversion in the European-Mediterranean area, *Orfeus Newsletter,* **2,** 5.

Braunmiller, J., Kradolfer, U., Baer, M. & Giardini, D., 2002. Regional moment tensor determination in the European-Mediterranean region—initial results, *Tectonophysics,* **356,** 5–22.

Davis, S.D. & Fröhlich, C., 1995. A comparison of moment tensor solutions in the Harvard CMT and USGS catalogues, *EOS, Trans. Am. geophys. Un.,* **76,** F381.

Dreger, D.S. & Helmberger, D.V., 1993. Determination of source parameters at regional distances with three-component sparse network data, *J. geophys. Res.,* **98,** 8107–8125.

Dreger, D.S., Ritsema, J. & Pasyanos, M., 1995. Broadband analysis of the 21 September, 1993, klamath falls earthquake sequence, *Geophys. Res. Lett.,* **105,** 997–1000.

Dziewonski, A.M. & Anderson, D.L., 1981. Preliminary reference earth model, *Phys. Earth planet. Inter.,* **25,** 297–356.

Dziewonski, A.M. & Woodhouse, J.H., 1983. An experiment in systematic study of global seismicity: centroid-moment tensor solutions for 201 moderate and large earthquakes of 1981, *J. geophys. Res.,* **88,** 3247–3271.

Dziewonski, A.M., Chou, T.-A. & Woodhouse, J.H., 1981. Determination of earthquake source parameters from waveform data for studies of global and regional seismicity, *J. geophys. Res.,* **86,** 2825–2852.

Fröhlich, C., 1994. Earthquakes with non-double-couple mechanisms, *Science,* **264,** 804–809.

Fröhlich, C., Millard, F.C., Massel, C. & Mann, P., 1997. Constraints on macquarie tectonics provided by harvard focal mechanisms and teleseismic earthquake locations, *J. geophys. Res.,* **102,** 5029–5041.

Giardini, D., 1992. Moment tensor inversion from mednet data (1). Large worldwide earthquakes of 1990, *Geophys. Res. Lett.,* **19,** 713–716.

Giardini, D., Boschi, E. & Palombo, B., 1993a. Moment tensor inversion from mednet data (2). Regional earthquakes of the Mediterranean, *Geophys. Res. Lett.,* **20,** 273–276.

Giardini, D., Palombo, B. & Boschi, E., 1993b. The determination of earthquake size and source geometry in the Mediterranean Sea, in *Recent evolution and seismicity of the Mediterranean area,* eds Boschi, E., Mantovani, E. & Morell, A., pp. 213–238, Kluwer, Dordrecht.

Helffrich, G.R., 1997. How good are routinely determined focal mechanisms? Empirical statistics based on a comparison of Harvard, USGS and ERI moment tensors, *Geophys. J. Int.,* **131,** 741–750.

Henry, C., Woodhouse, J.H. & Das, S., 2002. Stability of earthquake moment tensor inversions: effect of the double-couple constraint, *Tectonophysics,* **356,** 115–124.

Jackson, J.A. & McKenzie, D., 1988. The relationship between plate motions and seismic moment tensor, and the rates of active deformation in the Mediterranean and Middle East, *Geophys. J.,* **93,** 45–73.

Kanamori, H., 1977. The energy release in great earthquakes, *J. geophys. Res.,* **82,** 2981–2987.

Kawakatsu, H., 1995. Automated near-realtime CMT inversion, *Geophys. Res. Lett.,* **22,** 2569–2572.

Kradolfer, U., 1996. Autodrm—the first five years, *Seis. Res. Lett.,* **67,** 30–33.

Kubo, A., Fukuyama, E. & Nonomura, K., 2002. NIED seismic moment tensor catalogue for regional earthquakes around Japan: quality test and application, *Tectonophysics,* **356,** 23–48.

Kuge, K. & Kawakatsu, H., 1993. Significance of non-double couple components of deep and intermediate-depth earthquakes: implications from moment tensor inversion of long-period seismic waves, *Phys. Earth planet. Inter.,* **75,** 243–266.

Kuge, K. & Lay, T., 1994. Data-dependent non-double-couple components of shallow earthquake source mechanisms: Effects of waveform inversion instability, *Geophys. Res. Lett.,* **21,** 9–12.

Larson, E.W. & Ekström, G., 2001. Global models of surface wave group velocity, *Pure appl. Geophys.,* **158,** 1377–1399.

Nábělek, J. & Xia, G., 1995. Moment-tensor analysis using regional data: application to the 25 March, 1993, Scotts Mills, Oregon, earthquake, *Geophys. Res. Lett.,* **22,** 13–16.

Pasyanos, M.E., Dreger, D.S. & Romanowicz, B., 1996. Toward real-time estimation of regional moment tensors, *Bull. seism. Soc. Am.,* **86,** 1255–1269.

Pasyanos, M.E., Walter, W.R. & Hazler, S.E., 2001. A surface wave dispersion study of the Middle East and North Africa for monitoring the comprehensive nuclear-test-ban treaty, *Pure appl. Geophys.,* **158,** 1445–1474.

Patton, H. & Aki, K., 1979. Bias in the estimate of seismic moment tensor by the linear inversion method, *Geophys. J. R. astr. Soc.,* **59,** 479–495.

Pondrelli, S., Morelli, A., Ekström, G., Mazza, S., Boschi, E. & Dziewonski, A.M., 2002. European-Mediterranean regional centroid-moment tensors: 1997–2000, *Phys. Earth planet. Inter.,* **130,** 71–101.

Ritsema, J. & Lay, T., 1993. Rapid source mechanism determination of large ($M_w \geq 4.5$) earthquakes in western United States, *Geophys. Res. Lett.,* **20,** 1611–1614.

Romanowicz, B., Dreger, D., Pasyanos, M. & Uhrhammer, R., 1993. Monitoring strain release in central and northern California using broadband data, *Geophys. Res. Lett.,* **20,** 1643–1646.

Sicilia, D., 1999. Towards regional moment tensor determination: the moment tensor of the 1994 mb = 4.8 event near the Balearic Islands and its uncertainties, *MSc thesis*, ETH Zürich.

Šílený, J. & Vavryčuk, V., 2002. Can unbiased source be retrieved from anisotropic waveforms by using an isotropic model of the medium?, *Tectonophysics,* **356,** 125–138.

Sipkin, S.A., 1982. Estimation of earthquake source parameters by the inversion of waveform data: synthetic waveforms, *Phys. Earth planet. Inter.,* **30,** 242–259.

Sipkin, S.A., 1986. Estimation of earthquake source parameters by the inversion of waveform data: global seismicity, 1981–1983, *Bull. seism. Soc. Am.,* **76,** 1515–1541.

Stich, D., Ammon, C.J. & Morales, J., 2003. Moment tensor solutions for small and moderate earthquakes in the ibero-maghreb region, *J. geophys. Res.,* **108**(B3), 2148, doi:10.1029/2002JB002057.

Thio, H.-K. & Kanamori, H., 1995. Moment tensor inversion for local earthquakes using surface waves recorded at terrascope, *Bull. seism. Soc. Am.,* **85,** 1021–1038.

van der Lee, S., 1998. Observation and origin of Rayleigh-wave amplitude anomalies, *Geophys. J. Int.,* **135,** 691–699.

van Eck, T., Dost, B. & Hanka, W., 2001. European scale real-time waveform data exchange, *EMSC Newsletter,* **17,** 11.

Wessel, P. & Smith, W.H.F., 1995. New version of the generic mapping tool released, *EOS Trans. Am. geophys. Un.,* **76,** 329.

Woodhouse, J.H., 1988. The calculation of eigenfrequencies and eigenfunctions of the free oscillations of the Earth and the Sun, in *Seismological Algorithms,* ed. Doornbos, D.J., pp. 321–370, Academic Press, London.

Zhang, J. & Lay, T., 1990. Effects of centroid location on determination of earthquake mechanisms using long-period surface waves, *Bull. seism. Soc. Am.,* **80,** 1205–1231.